arXiv:1510.03049v1 [cond-mat.mtrl-sci] 11 Oct 2015

Crystal Field Excitations in Breathing Pyrochlore Antiferromagnet $Ba_3Yb_2Zn_5O_{11}$

T. Haku[1], M. Soda[1], M. Sera[2], K. Kimura[2], S. Itoh[3], T. Yokoo[3], T. Masuda[1]
[1] *Institute for Solid State Physics, The University of Tokyo, Kashiwa, Chiba 277-8581, Japan*
[2] *Division of Materials Physics, Graduate School of Engineering Science, Osaka University, Toyonaka, Osaka 560-8531, Japan*
[3] *Institute of Materials Structure Science, High Energy Accelerator Research Organization, Tsukuba, Ibaraki 305-0801, Japan*

Inelastic neutron scattering measurement is performed on a breathing pyrochlore antiferromagnet $Ba_3Yb_2Zn_5O_{11}$. The observed dispersionless excitations are explained by a crystalline electric field (CEF) Hamiltonian of Kramers ion Yb^{3+} of which the local symmetry exhibits C_{3v} point group symmetry. The magnetic susceptibility previously reported is consistently reproduced by the energy scheme of the CEF excitations. The obtained wave functions of the ground state Kramers doublet exhibit the planer-type anisotropy. The result demonstrates that $Ba_3Yb_2Zn_5O_{11}$ is an experimental realization of breathing pyrochlore antiferromagnet with a pseudospin $S = 1/2$ having easy-plane anisotropy.

I. INTRODUCTION

Geometrical frustration in magnetic materials disturbs the development of long-range order and induces novel states at low temperatures.[1,2] A three-dimensional network of corner-sharing tetrahedra, i.e., the pyrochlore lattice, is one of the most interesting systems. The geometrical configuration prohibits the arrangement of the spins that satisfy the lowest energy of all spin bonds, leading to the ground state sensitive to perturbations including single-ion anisotropy, two-ion anisotropy, and lattice distortion. Indeed the variety of the magnetic phases have been reported in rare-earth pyrochlore compounds in $R_2Ti_2O_7$.[3] In case of R = Dy and Ho spin-ice states emerge[4] due to the geometrical frustration induced by ferromagnetic interaction and the Ising anisotropy.[5–8] In contrast in $Yb_2Ti_2O_7$ the easy-plane type anisotropy of Yb ion enhances quantum effect, leading to quantum spin liquid state.[9]

In a series of pyrochlore titanates $R_2Ti_2O_7$ rare earth ions carry magnetic moment. The J multiplets of the ions are lifted by crystalline electric field (CEF) from octahedral ligands with the point symmetry D_{3d}. In case of R = Dy, Ho, and Yb, the ground state is doublet and the first excited energies are larger than 20 meV,[4] meaning that the degree of freedom of the magnetic moments are approximately two in the temperature range of $T << 200$ K. The magnetic moments are, thus, regarded as pseudospins $S = 1/2$ with anisotropies determined by the wave functions of the ground state. In most cases the localized orbitals of f-electrons give small magnetic interactions, and, therefore, rare-earth magnets can be interacting spin systems at low temperatures. Since the spin anisotropy is one of key features for the emerged magnetic state, experimental study on CEF is crucial particularly for the initial stage of the research on rare-earth magnets.

Breathing pyrochlore lattice, i.e., alternating arrays of corner-sharing large and small tetrahedra, is interesting in terms of realization of the perturbative expansion method in theoretical calculation.[10] The original model compounds were reported in 3*d*-transition metal spinels $LiInCr_4O_8$ and $LiGaCr_4O_8$.[11] Recently rare-earth-based compound was found in $Ba_3Yb_2Zn_5O_{11}$ where Kramers ion Yb^{3+} carries pseudospin $S = 1/2$.[12] Fig. 1(a) shows the breathing pyrochlore network of Yb^{3+} ions. Distances between Yb^{3+} ions of small and large tetrahedra are 3.3 Å and 6.2 Å, respectively.

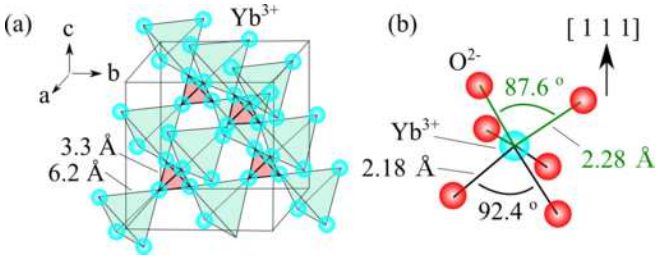

FIG. 1. Crystal structure of $Ba_3Yb_2Zn_5O_{11}$. (a) Breathing pyrochlore network of Yb^{3+} ions. (b) Local structure of YbO_6, which has C_{3v} symmetry. The symmetry axis is [1 1 1].

The space group is $F\bar{4}3m$ with cubic symmetry. The local structure of YbO_6 is a distorted octahedron with the C_{3v} point group symmetry as shown in Fig. 1 (b).

No phase transition were observed in the specific heat and magnetic measurement in 0.4 K $< T <$ 300 K. A temperature dependence of the magnetic susceptibility was reasonably reproduced using cubic symmetry for the CEF Hamiltonian down to 30 K, even though YbO_6 originally exhibited lower symmetry. This indicated that local distortion of a YbO_6 octahedron is small enough to be approximated as a structure with cubic symmetry. It has been reported that the ground state of CEF Hamiltonian is a Kramers doublet, and that the first excited state is a quartet state having an excitation energy of $E = 45.1$meV[12]. Up to room temperature, the excitation energy is sufficiently high so that Yb^{3+} moment is regarded as an isotropic pseudospin $S = 1/2$. The bulk magnetic properties in the low temperatures were explained by the presumed isotropic Heisenberg $S = 1/2$ model having nonmagnetic ground state. For the further understanding of the ground state, however, the information of the spin anisotropy is important and, therefore, the investigation on the CEF is indispensable.

In the present study, we performed inelastic neutron (INS) scattering measurement to identify the precise CEF Hamiltonian. Three excitations were observed at $\hbar\omega = 38.2, 55.0$ and 68.3 meV, and all were qualitatively consistent with the energy spectrum of the C_{3v} point group of the local YbO_6 structure, consisting of four Kramers doublets. The energy of the first excited state is consistent with that estimated by

the magnetic susceptibility measurement, such that Yb^{3+} ions are regarded as the ion having pseudospin $S = 1/2$ at low temperatures. The C_{3v} symmetry leads to the anisotropic ground state wave functions with the spin anisotropy of $q = 3.31$ for $J_{xy} = qS_{xy}$ and $p = 2.35$ for $J_z = pS_z$, where $\boldsymbol{J}$ is total angular momentum and $\boldsymbol{S}$ is effective spin $S = 1/2$ operator.

II. EXPERIMENTAL DETAILS

The inelastic neutron scattering measurement (INS) was performed by using high resolution chopper spectrometer (HRC) installed in J-PARC/MLF. We used 17.7 g powder sample synthesized by a solid state reaction method. The sample was set in an Al-can filled with exchange He gas. Measurements were performed at $T = 3$, 200 and 300 K using an ^{4}He-type closed-cycle refrigerator. The T_0 chopper for the elimination of fast neutrons was set at 50 Hz and a collimator of 1.5° was installed in front of sample. The initial neutrons were monochromated by type "S" Fermi chopper with the frequency of 600 Hz to obtain the neutron energy of $E_i = 154.4$ meV with the instrumental resolution (full width at half maximum, FHWM) of 5.5 meV at the elastic position. Preliminary INS measurement with $E_i = 150$ meV was performed at MARI specrometer installed in ISIS.

III. RESULTS

Figure 2(a), (b), and (c) show contour maps of the INS spectrum at $T = 3$, 200, and 300 K, respectively. The arrows indicate three dispersionless excitations at $\hbar\omega = 38.2, 55.0$ and 68.3 meV. The intensities of these excitations decrease with the increase of Q, and they decrease with the increase of the temperature. None of the excitation-energy values changes in the observed temperature range. These behaviors are consistent with that of excitations of a magnetic cluster. At $\hbar\omega \lesssim 30$meV we observed broad excitation of which the intensity increases with the Q, and it increases with the temperature. The excitation is, thus, regarded as phonons. At $\hbar\omega \sim 100$ meV flat stripe is observed in Fig. 2(a). Since no intensity was observed at 100 meV in preliminary measurement at MARI (not shown), the stripe is regarded as artifact.

Figure 3(a) shows the Q dependences of the intensities of the three modes. The data are obtained by integrating the intensities in the ranges of 32 meV $\leq \hbar\omega \leq$ 44 meV, 44 meV $\leq \hbar\omega \leq$ 64 meV, and 64 meV $\leq \hbar\omega \leq$ 72 meV. The intensities decrease with the increase of Q, and they follow the magnetic form factor of the Yb^{3+} ion indicated by the solid curves.[14] These excitations, thus, derive from the CEF of the Yb^{3+} ion.

The symbols shown in Fig. 3(b), 3(c), and 3(d) indicate $\hbar\omega$ dependence of the integrated intensities at $T = 3$, 200, and 300 K, respectively, where the integral range is 2.8 $Å^{-1} \leq Q \leq 3.2Å^{-1}$. The phonon contributions have been subtracted by assuming that the intensity is proportional to Q^2 and also to the Bose factor. The intensities of the three modes decrease with the increase of the temperature. Since

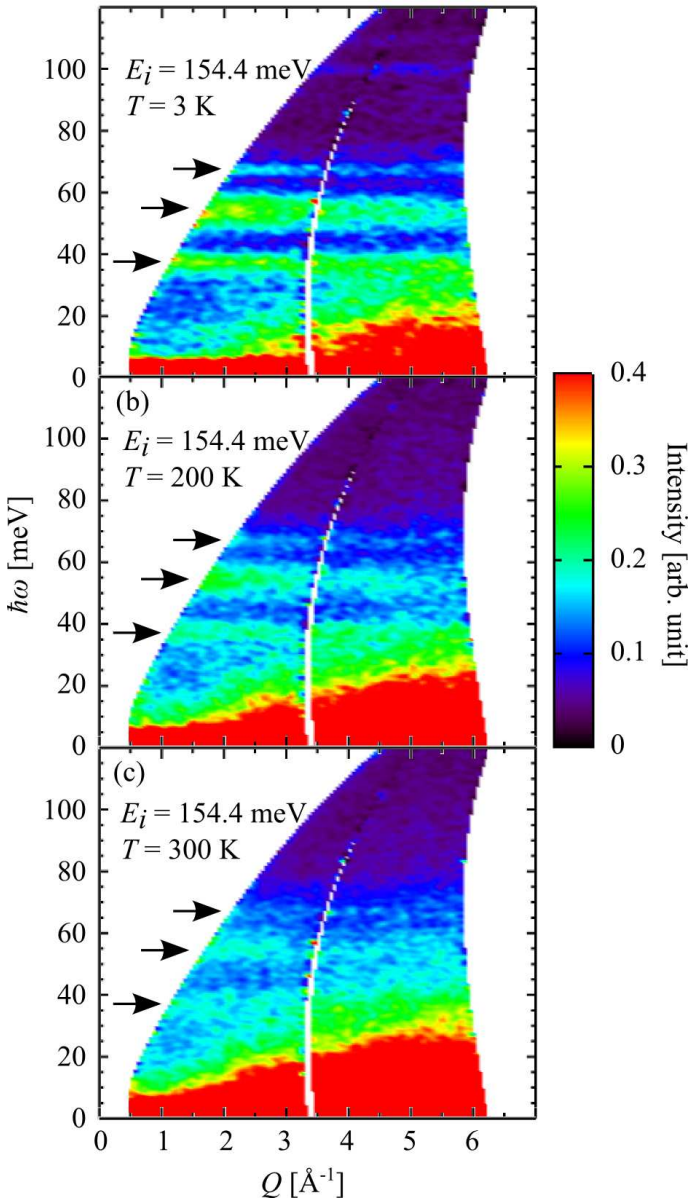

FIG. 2. Contour plots of inelastic neutron spectra measured at at (a)$T = 3$, (b)$T = 200$, and (c)$T = 300$ K. The arrows indicate dispersionless excitations at $\hbar\omega$ = 38.2, 55.0 and 68.3 meV.

the occupancy of the ground state decreases with the increase of the temperature and the occupancy is one of coefficients in magnetic neutron cross section, all of the excitations derive from the transitions between the ground state and excited states. This means that the Yb^{3+} ion is the four level system as described by solid bars in the first row in Fig. 4(a). The result is in contrast with the three level system assumed in the previous study[12] as described by dotted bars in the second row. The first excited energy of the present study is, however, close to that of previous one. This means that the assumption of pseudospin $S = 1/2$ for the Yb^{3+} ion[12] is good in the low temperatures.

The three peaks at T = 3 K in Fig. 3(b) are fit by Gaussian functions, and the integrated intensities will be used to compare the calculation in the next section. The estimated FWHMs at $\hbar\omega$ = 38.2, 55.0, and 68.3 meV are $\Delta\hbar\omega$ = 5.5, 8.9 and 3.9 meV, respectively. The FWHM at 55.0 meV is wider than the instrumental energy resolution. This indicates that there is either a lowering of symmetry in the local structure of YbO_6 or a coupling of CEF and phonon excitations. In addition, at T = 200 and 300 K, the peaks widthes bcome broadened. This indicates that the relaxation of the CEF excitation is enhanced thorough the coupling with lattice.[13]

IV. DISCUSSIONS

The obtained energy diagrams of $Ba_3Yb_2Zn_5O_{11}$ is different from that of simple cubic symmetry for the local structure around Yb^{3+} ion assumed in a previous study.[12] Instead the diagram is similar to the case of oxides of which the local structure is distorted, $Yb_2Ti_2O_7$ or $YbBa_2Cu_3O_7$, where the first excited states with fourfold degeneracy in the cubic symmetry are lifted into a pair of doublets. We, hence, analyze the CEF excitation based on the precise ligand symmetry, C_{3v}, in $Ba_3Yb_2Zn_5O_{11}$.

The CEF Hamiltonian is as follows,

$$\mathcal{H}_{CEF} = B_2^0 O_2^0 + B_4^0 O_4^0 + B_4^3 O_4^3 + B_6^0 O_6^0 + B_6^3 O_6^3 + B_6^6 O_6^6, \quad (1)$$

where B_m^n and O_m^n are CEF parameters and Steven's operators, respectively.[16,17] The neutron cross section of the CEF excitations is, according to the dipole approximation,[18]

$$I_{calc}(\boldsymbol{\kappa}, \hbar\omega) = r_0^2 \frac{k'}{k} \sum_{\alpha,\beta=x,y,z} (\delta_{\alpha\beta} - \hat{\kappa}_\alpha \hat{\kappa}_\beta) F^2(\kappa) \times p_\lambda \langle\lambda|J_\alpha|\lambda'\rangle \langle\lambda'|J_\beta|\lambda\rangle \, \delta(\hbar\omega - E_{\lambda'} + E_\lambda). \quad (2)$$

Here $\boldsymbol{\kappa}$ is scattering vector, and $\hat{\boldsymbol{\kappa}}$ is the normalized one. The initial and final states of the CEF excitations are denoted by $|\lambda\rangle$ and $|\lambda'\rangle$. The probability of state $|\lambda\rangle$ is represented as p_λ. $F(\kappa)$ is the magnetic form factor.[14] The value of r_0 is -0.54×10^{-15} m. Powder averaged intensity $I_{\rm calc}^{\rm powder}(\kappa, \hbar\omega)$ is obtained in order to compare the calculation to the experimental data. The integrated intensities for three modes at T = 3 K obtained in Fig. 3(b) are fit by $I_{\rm calc}^{\rm powder}(\kappa, \hbar\omega)$. The solid curves are $I_{\rm calc}^{\rm powder}(\kappa, \hbar\omega)$ convoluted by Gaussian functions having FWHMs obtained in previous section. The fit to the data is reasonable. The obtained CEF parameters are summarized in Table I. The wave functions of the ground states are

$$|\pm\rangle = \mp 0.537 \, |\pm\frac{7}{2}\rangle - 0.805 \, |\pm\frac{1}{2}\rangle \pm 0.251 \, |\mp\frac{5}{2}\rangle. \quad (3)$$

The solid curves in Figs. 3(c) and 3(d) are the calculation using the obtained CEF parameters. Since the peaks are broadened with the increase of the temperature, we take the FWHMs for the peaks as fitting parameters. The calculation

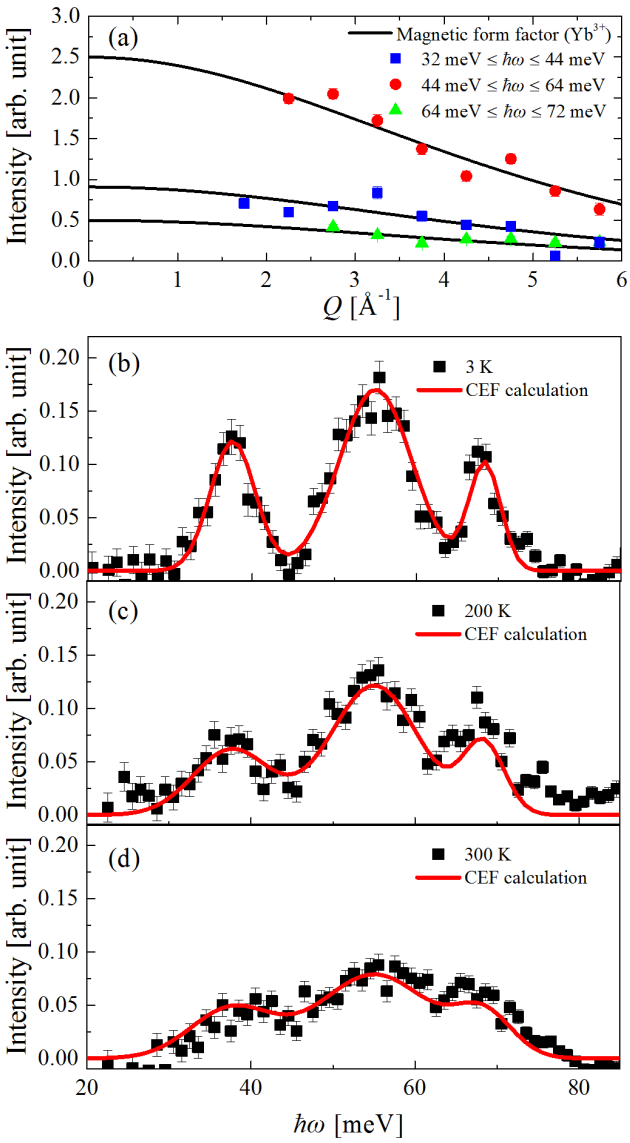

FIG. 3. (a) Q dependence of neutron intensities for three modes. The symbols are the data obtained by integrating the intensities in the ranges of 32meV ≤ $\hbar\omega$ ≤ 44meV, 44meV ≤ $\hbar\omega$ ≤ 64meV and 64meV ≤ $\hbar\omega$ ≤ 72meV at T = 3 K. The solid curves show the Q dependence of the magnetic form factor of Yb^{3+} in Ref. 14. The symbols of (b), (c) and (d) show the $\hbar\omega$ dependences of the neutron intensities at T = 3, 200 and 300 K. The intensities are integrated in the range of 2.8Å^{-1} ≤ Q ≤ 3.2Å^{-1}. The red curves show the calculations (see the text).

reasonably reproduces the data. When a trigonal axis of the YbO_6 structure is chosen as a quantization axis and a pseudospin operator $\boldsymbol{S}$ is defined as $J_x = qS_x$, $J_y = qS_y$, $J_z = pS_z$, p and q are as follows,

$$\pm\frac{1}{2}p = \langle\pm|J_z|\pm\rangle = \pm\frac{1}{2} \times 2.35 \quad (4)$$

$$q = \langle\pm|J_\pm|\mp\rangle = 3.31. \quad (5)$$

The result means that a wave function of the ground state has

TABLE I. Values for B_n^m of $Ba_3Yb_2Zn_5O_{11}$ obtained by INS experiment in the present study and those by the magnetic susceptibility measurement in the previous study.[12]

	B_2^0	$B_4^0 \times 10^2$	$B_4^3 \times 10^2$	$B_6^0 \times 10^4$	$B_6^3 \times 10^4$	$B_6^6 \times 10^4$
Present study (meV)	0.0737	−2.76	−33.6	6.10	8.70	88.2
Previous study (meV)	0	3.45	−97.4	3.06	37.9	29.5

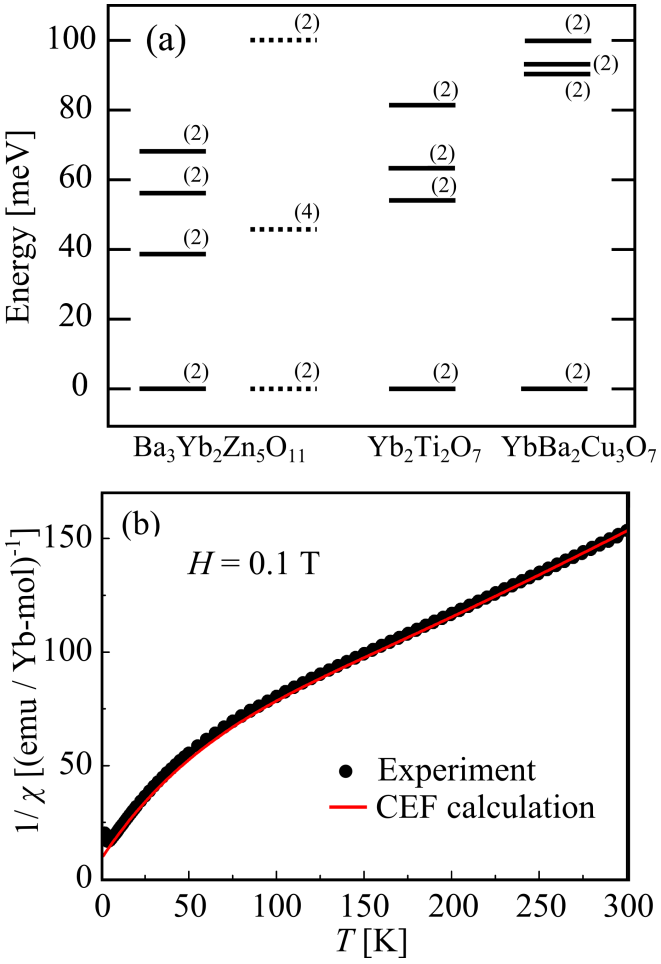

FIG. 4. (a) Energy diagrams of Yb^{3+} compounds, $Ba_3Yb_2Zn_5O_{11}$[12], $Yb_2Ti_2O_7$[4] and $YbBa_2Cu_3O_7$[15]. The solid and dotted lines indicate the levels obtained by neutron scattering studies and bulk measurement, respectively. (b) Magnetic susceptibility curve at H = 0.1 T. The solid circles are the experimental values cited in ref. 16. The solid curve is a calculated value using the parameter set from the first line of Table I and an antiferromagnetic molecular field constant $\lambda = -9$ emu/mol.

planar-type anisotropy.

The magnetic susceptibility χ is calculated as follows.[19]

$$\chi = \chi_{dia} + \chi_{CEF}/(1 - \lambda\chi_{CEF}) \quad (6)$$

Here χ_{CEF} is the magnetic susceptibility determined by the CEF Hamiltonian. χ_{dia} is the diamagnetic susceptibility fixed to be -4×10^{-4}emu/mol-Yb. λ is a molecular field constant defined as $\boldsymbol{H}_{eff} = \boldsymbol{H} + \lambda\boldsymbol{M}$, where $\boldsymbol{H}$, $\boldsymbol{M}$ and $\boldsymbol{H}_{eff}$ are an external field, magnetization and an effective molecular field, respectively. The solid curve in Fig. 4 (b) is the calculated one with the parameters obtained by the present INS experiment and an antiferromagnetic molecular field constant $\lambda = -9$ mol/emu. The experimental data are from Ref. 12. The calculation reasonably reproduced the experimental data. The CEF parameter obtained by INS experiment reproduces the magnetic susceptibility measured independently.

V. CONCLUSION

We performed a neutron scattering experiment on a powder sample of $Ba_3Yb_2Zn_5O_{11}$ in order to identify the CEF Hamiltonian. The neutron spectrum was explained by four Kramers doublets of Yb^{3+} ion. The obtained CEF parameters revealed that the Yb^{3+} ions are regarded as the pseudospin $S = 1/2$ having easy-plane anisotropy. Next challenge is further investigation on the low-energy spin dynamics of the breathing pyrochlore spin system by using a cold neutron spectrometer.

ACKNOWLEDGEMENTS

T. Haku was supported by the Japan Society for the Promotion of Science through the Program for Leading Graduate Schools (MERIT). This work was supported by JSPS KAKENHI Grant in Aid for Scientific Research (B) Grant No. 24340077. The neutron scattering experiment at HRC spectrometer in KEK was approved by the Neutron Scattering Program Advisory Committee of IMSS, KEK (Proposal No. 2013S01 and 2014S01) and ISSP. Preliminary neutron experiment was performed at MARI spectrometer in ISIS, Rutherford Appleton Laboratory. Dr. J. Taylor is greatly appreciated for his experimental support at MARI. Travel expenses for the experiment performed using MARI at ISIS, UK, were supported by General User Program for Neutron Scattering Experiments, Institute for Solid State Physics, The University of Tokyo (proposal no. 14522), at JRR-3, Japan Atomic Energy Agency, Tokai, Japan.

[1] A. P. Ramirez, Annu. Rev. Mater. Sci. **24**, 453 (1994).
[2] L. Balents, Nature **464**, 199 (2010).
[3] J. S. Gardner, M. J. P. Gingras, and J. E. Greedan, Rev. Mod. Phys. **82**, 53 (2010).
[4] A. Bertin, Y. Chapuis, P. D. Reothier, and A. Yaouane, J. Phys.:Condens. Matter **24**, 256003 (2012).
[5] A. P. Ramirez, A. Hayashi, R. J. Cava, R. Siddharthan, and B. S. Shastry, Nature **399**, 333 (1999).
[6] S. Rosenkranz, A. P. Ramirez, A. Hayashi, R. J. Cava, and R. Siddharthan, J. Appl. Phys. **87**, 5914 (2000).
[7] M. J. Harris, S. T. Bramwell, T. Zeiske, D. F. Mcmorrow, and P. J. C. King, J. Magn. Magn. Mater. **177**, 757 (1998).
[8] S. T. Bramwell, M. J. Harris, B. C. den Hertog, and et al.,Phys. Rev. Lett. **87**, 047205 (2001).
[9] K. A. Ross, L. Savary, B. Gaulin, and L. Balents, Phys.Rev. X **1**, 021002 (2011).
[10] H. Tsunetsugu, Phys. Rev. B **65**, 024415 (2001).
[11] Y. Okamoto, G. J. Nilsen, J. P. Attfield, and Z. Hiroi, Phys. Rev. Lett. **110**, 097203 (2012).
[12] K. Kimura, S. Nakatsuji, and T. Kimura, Phys. Rev. B **90**, 060414 (2014).
[13] S. W. Lovessy and U. Staub, Phys. Rev. B **61**, 9130 (2000).
[14] P. J. Brown, *International tables for crystallography* (John Wiley and Sons, Inc, 2006) 1st online ed., Vol. C, p. 454.
[15] M. Guillaume, P. Allenspach, J. Mesot, U. Staub, A. Furrer, R. Osborn, A. D. Taylor, F. Stucki, and P. Unternhrer, Solid State Commun. **81**, 999 (1992).
[16] M. J. Hutchings, Solid State Phys. **16**, 227 (1964).
[17] K. W. H. Stevens, Proc. Phys. Soc., Sect. A Proc. **65**,209 (1952).
[18] S. W. Lovesey, *Theory of neutron scattering from condensed matter* (Clarendon Press, Oxford, U.K., 1984) Vol. 2, p. 242.
[19] J. H. V. Vleck, *The Theory of Electronic and Magnetic Susceptibilities* (Ocford University Press, Oxford, U.K., 1932) p. 245.